Article

SnS$_2$/TiO$_2$ Nanocomposites for Hydrogen Production and Photodegradation under Extended Solar Irradiation

Sivagowri Shanmugaratnam [1,2], Balaranjan Selvaratnam [3], Aravind Baride [3], Ranjit Koodali [4,*], Punniamoorthy Ravirajan [1], Dhayalan Velauthapillai [2] and Yohi Shivatharsiny [5,*]

1   Clean Energy Research Laboratory (CERL), Department of Physics, University of Jaffna, Jaffna 40000, Sri Lanka; sivagowrishanmugaratnam@gmail.com (S.S.); pravirajan@univ.jfn.ac.lk (P.R.)
2   Faculty of Engineering and Science, Western Norway University of Applied Sciences, P.O. Box 7030, 5020 Bergen, Norway; Dhayalan.Velauthapillai@hvl.no
3   Department of Chemistry, University of South Dakota, Vermillion, SD 57069, USA; Balaranjan.Selvaratn@coyotes.usd.edu (B.S.); Aravind.Baride@usd.edu (A.B.)
4   Western Kentucky University, 1906 College Heights Blvd, Bowling Green, KY 42101, USA
5   Department of Chemistry, University of Jaffna, Jaffna 40000, Sri Lanka
*   Correspondence: Ranjit.Koodali@wku.edu (R.K.); yshiva@univ.jfn.ac.lk (Y.S.); Tel.: +94-773644036 (Y.S.)

Abstract: Earth–abundant transition metal chalcogenide materials are of great research interest for energy production and environmental remediation, as they exhibit better photocatalytic activity due to their suitable electronic and optical properties. This study focuses on the photocatalytic activity of flower-like SnS$_2$ nanoparticles (composed of nanosheet subunits) embedded in TiO$_2$ synthesized by a facile hydrothermal method. The materials were characterized using different techniques, and their photocatalytic activity was assessed for hydrogen evolution reaction and the degradation of methylene blue. Among the catalysts studied, 10 wt. % of SnS$_2$ loaded TiO$_2$ nanocomposite shows an optimum hydrogen evolution rate of 195.55 μmolg^{-1}, whereas 15 wt. % loading of SnS$_2$ on TiO$_2$ exhibits better performance against the degradation of methylene blue (MB) with the rate constant of 4.415×10^{-4} s^{-1} under solar simulated irradiation. The improved performance of these materials can be attributed to the effective photo-induced charge transfer and reduced recombination, which make these nanocomposite materials promising candidates for the development of high-performance next-generation photocatalyst materials. Further, scavenging experiments were carried out to confirm the reactive oxygen species (ROS) involved in the photocatalytic degradation. It can be observed that there was a 78% reduction in the rate of degradation when IPA was used as the scavenger, whereas around 95% reduction was attained while N$_2$ was used as the scavenger. Notably, very low degradation (<5%) was attained when the dye alone was directly under solar irradiation. These results further validate that the •OH radical and the superoxide radicals can be acknowledged for the degradation mechanism of MB, and the enhancement of degradation efficiency may be due to the combined effect of in situ dye sensitization during the catalysis and the impregnation of low bandgap materials on TiO$_2$.

Keywords: photocatalyst; hydrothermal; hydrogen evolution; degradation; transition metal chalcogenide; TiO$_2$; SnS$_2$

1. Introduction

Emission-less, energy efficient, and low-carbon power production is vital for a green economy. Therefore, renewable energy production from hydro, wind, and solar power paves the way toward overcoming the current environmental issues of fossil fuels [1]. Photocatalytic water splitting involved in hydrogen and oxygen evolution reactions can produce chemical energy in H$_2$ and O$_2$ by utilizing solar energy [2]. The practical application of overall water splitting remains limited due to the lack of effective and stable

catalysts to reduce reaction energy barriers. Therefore, the development of efficient and affordable photocatalysts is of great significance.

Various materials, such as TiO_2 [3–6], ZnO [7], mixed oxide materials [8], dye [9,10], and metal-doped oxide materials [11,12], have been intensively focused on for photocatalytic applications. Among these, TiO_2 is considered a gold standard due to its significant characteristics, such as strong optical absorption, favorable band edge position, nontoxicity, and abundant availability [13,14]. However, the wide bandgap energy (~3.2 eV) of TiO_2 necessitates UV irradiation, but the composites of TiO_2 with co-catalysts enable the catalysts to absorb visible light abundant in solar radiation [15].

Recently, transition metal chalcogenides (TMCs) have gained more attention due to their electrocatalytic properties that includes indirect bandgaps, optoelectronic behavior, and their stability [16,17]. Moreover, the stronger edge effects and the quantum confinement effects make these nanodots (quantum dots) or nanostructures of metal chalcogenides possible to utilize considerable amounts of solar irradiation [17–19]. These are playing an increasingly important role in different applications, such as photo degradation [20], capacitors [21], and hydrogen evolution [22] due to their suitable electronic and optical properties.

The generation of an exciton pair and the effective charge separation in these semiconductor photocatalysts lead to an efficient photocatalytic process. The efficiency of charge transport mainly depends on the crystallinity, particle, and crystallite size of the materials. Although the small bandgap energy of TMCs necessitates the use of visible irradiation, composites of TMCs with co-catalysts, for example, graphene [23], graphene oxides [24], carbon nitride [25], metal oxides [26,27], and metals [28], were found to increase the conductivity of electrons, provide active sites, and effectively separate the electron and hole pairs generated by the semiconductor photocatalysts. Among the transition metal chalcogenides, SnS_2 receives significant attention due to its interesting optical and electronic properties [29]. It has a CdI_2-type layered n-type semiconductor and a bandgap of about 2.18 eV [30,31]. Until now, different SnS_2 nanostructures with a range of morphologies have been prepared in various conditions, exhibiting intriguing physical and chemical properties; for example, well uniform nanoflake SnS_2 was synthesized by the hydrothermal method at 145 °C in 48 h by Feng et al. [32], whereas in a different study, Huijuan Geng et al. used Titon-X 100 as a surfactant to get hexagonal nanoflake SnS_2 [33]. However, the photocatalytic performance of SnS_2 is still considered unsatisfactory, and only few works have been reported on SnS_2 nanoparticles for photocatalytic water splitting and photodegradation. The objective of this paper is to investigate whether SnS_2/TiO_2 nanocomposite will enhance the photocatalytic hydrogen production and rate of degradation of organics. Herein, we report SnS_2-embedded TiO_2 nanocomposites synthesized by the facile hydrothermal method for photocatalytic hydrogen production and photocatalytic degradation of methylene blue under simulated solar irradiation. We also investigate the optimal loading weight percentage of SnS_2 in the nanocomposite for these applications. These results will be of enormous interest to the scientific community involved in material chemistry research, especially with metal chalcogenide materials for various photocatalysis applications.

2. Results

2.1. Characterization of Materials

The powder XRD pattern of pure SnS_2, TiO_2, and different weight percentages of SnS_2/TiO_2 (5, 10, 15, and 20) nanocomposites are illustrated in Figure 1. The peaks observed at the 2 theta value of 25.29, 37.88, 48.25, 53.74, 55.14, 62.71, 68.86, 70.30, and 75.06 for the TiO_2 material are due to (101), (004), (200), (105), (211), (204), (116), (220), and (215) diffraction planes of anatase phase of TiO_2 (JCPDS:00-004-0477), and the peaks at 2 theta values of 14.76, 27.97, 32.00, 41.79, 49.92, 52.41, 54.79, and 60.55 for pristine SnS_2 are due to (001), (100), (101), (102), (110), (111), (103), and (201) diffraction planes, which confirms the formation of SnS_2 (JCPDS:00-023-0677). A combination of SnS_2 and TiO_2 peaks observed with the 5, 10, 15, and 20 wt. % SnS_2/TiO_2 (ST-5, ST-10, ST-15, and ST-20, respectively) nanocomposite confirms good impregnation of SnS_2 on TiO_2.
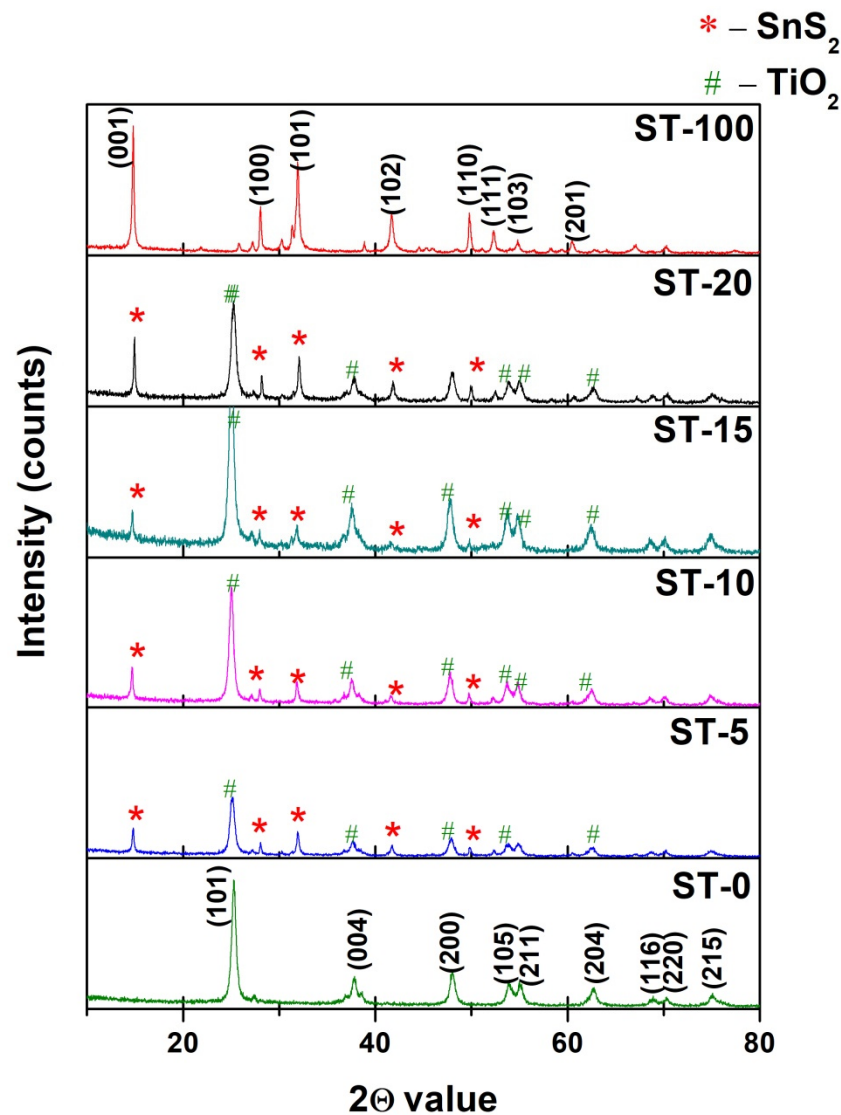
Figure 1. XRD for pristine TiO_2 (ST-0), SnS_2 (ST-100), and X wt. % of SnS_2/TiO_2 (ST-5, ST-10, ST-15, and ST-20) nanocomposites.

Scanning electron microscopic images of pristine TiO_2 and SnS_2 are illustrated in Figure 2a,b and Figure 2c,d, respectively. It can be clearly seen from Figure 2a,b that the pure TiO_2 nanoparticle showed an irregular 3D block-like structure covered with sponge-like particles. The micrograph obtained at higher magnification (Figure 2b) clearly illustrates that the aggregated particles have spongy-like structures, supported by the data published elsewhere [26]. A flower-like structure composed with nanosheets was attained for pristine SnS_2 and is shown in Figure 2c,d.

SEM images of different wt. % of SnS_2. embedded TiO_2 nanocomposites, ST-5 (e), ST-10 (f), ST-15 (g), and ST-20 (h), are shown in Figure 3. These SnS_2/TiO_2 nanocomposites in different wt. % possess nanosheets with a morphology decorated with sponge-like material and, therefore, exhibit aggregation.
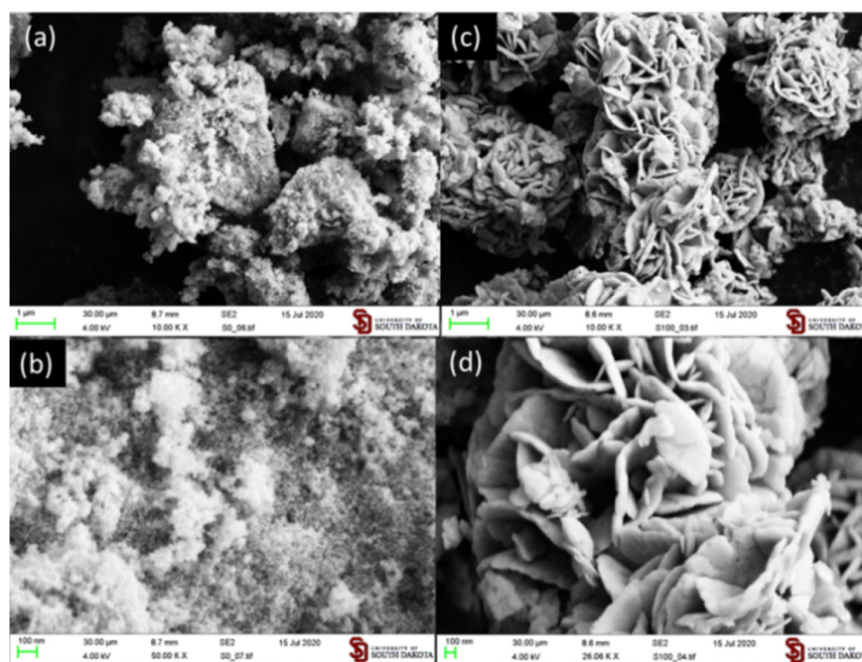
Figure 2. SEM images for (**a**,**b**): pristine TiO_2 (ST-0), and (**c**,**d**): SnS_2 (ST-100) nanomaterials.
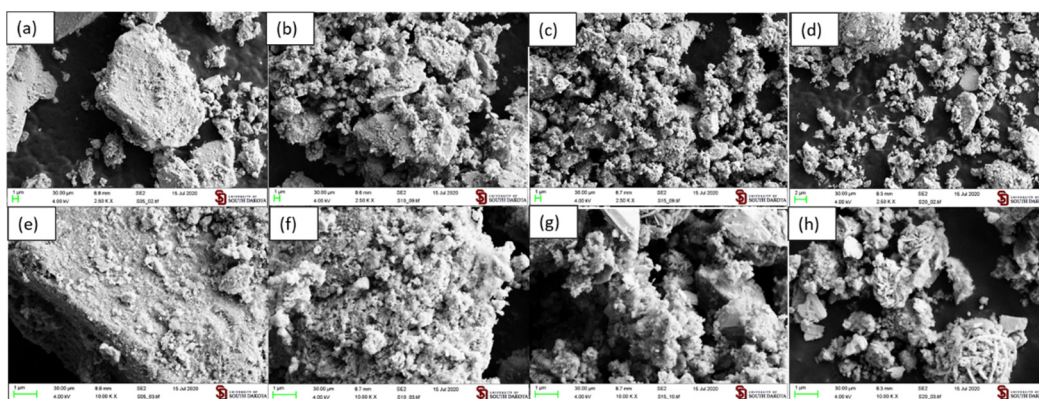

Figure 3. SEM images for X wt. % of SnS_2/TiO_2: (**a–e**) ST-5, (**b–f**) ST-10, (**c–g**) ST-15, and (**d–h**) ST-20 nanocomposites.

The atomic ratios between Sn and Ti were calculated by using energy dispersive spectroscopy (EDS), with the values found to be 0.029, 0.039, 0.052, and 0.101 for ST-5, ST-10, ST-15, and ST-20, respectively. The calculated values closely matched with the expected values, which are tabulated in Table S1.

The bandgap energies of the pristine SnS_2, and different wt. % of SnS_2/TiO_2 nanocomposite materials were estimated by using the Tauc plot (Figure 3), which transformed the absorption spectra (Figure 4a) via the Kubelka–Munk function [26,34], $[F(R\infty)E]^n$ vs. E, when n = 0.5, for a direct allowed transition (K = F(R∞)). Figure 4c shows the Tauc plot with the absorption spectra of pristine TiO_2. Bandgaps estimated from the Tauc plots, by extrapolating the steep portion of the plot in Figure 4b,c to the x-axis, suggest the bandgaps of pristine SnS_2 to be 1.890 eV, which is closer to some literature studies [35], and the bandgap values of SnS_2-embedded TiO_2 nanocomposite to be (ST-5—2.250 eV, ST-10—2.015 eV, ST-15—2.005 eV, and ST-20—1.980 eV), whereas the bandgaps for pristine TiO_2 (3.100 eV) materials lie in the range between 1.89 and 3.10 eV. The pure SnS_2 sample shows strong absorption in the visible region with an absorption edge of ~555 nm, corresponding to a bandgap of 1.89 eV. However, the loading of TiO_2 with SnS_2 elevates the absorption level/bandgap gradually, which is consistent with the visual color of the samples gradually changing from yellow to white.
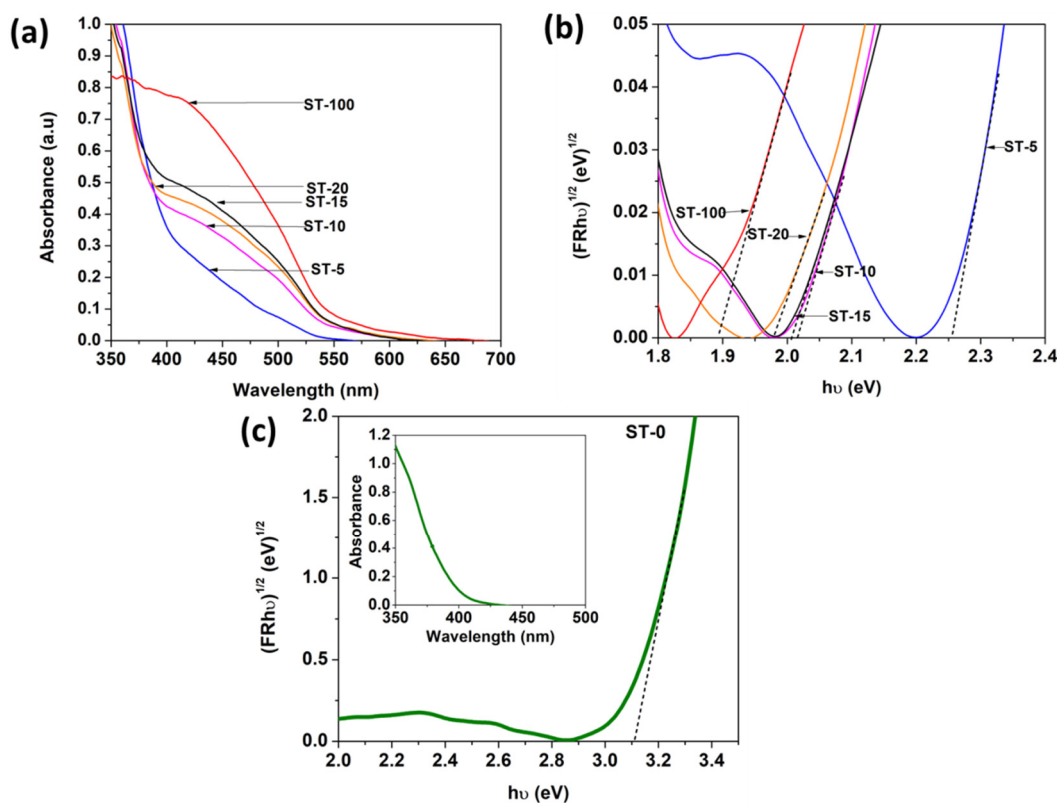
Figure 4. (**a**) Absorption spectra for samples ST-5, ST-10, ST-15, ST-20, and ST-100; (**b**) Tauc plot for S-5, ST-10, ST-15, ST-20, and ST-100 and; (**c**) Tauc plot of pure TiO_2 sample (ST-0) (inset shows the respective absorption spectra).

2.2. Photocatalytic Hydrogen Evolution

Transition metal chalcogenides (TMCs) have been in the spotlight due to their optoelectronic properties; in addition, they exhibit better performance against photocatalytic applications. To study SnS_2/TiO_2's activity for photocatalytic application, the synthesized nanocomposites for hydrogen production and photocatalytic dye degradation were used. The amount of H_2 evolution was measured under solar simulated illumination, and the results show an optimum hydrogen evolution of 195.55 µmolg^{-1} with 10 wt. % of SnS_2/TiO_2 nanocomposite, which is more than double the amount of hydrogen attained with pure TiO_2 (89.20 µmolg^{-1}), as presented in Table 2. The rate of hydrogen evolution was found to increase with increasing wt. % of SnS_2 on TiO_2 up to 10 wt. % of loading, and a further increase resulted with a decrease in hydrogen evolution. This result can be correlated with the bandgap energies of the materials, which may effectively induce the formation of electron–hole pairs. In the case of pure SnS_2 (Figure 5), there was no hydrogen evolution obtained; this can be related to the faster recombination of exciton pairs due to its relatively small bandgap energy (1.89 eV). These results may suggest that the SnS_2 nanoparticles act as a co-catalyst when they are in the SnS_2/TiO_2 nanocomposites and, thus, enhance excited electrons in the reactive site of titanium dioxide (Figure 7).

It is noteworthy to compare the result obtained in this study with the literature; although the experimental conditions are varied and the results are attained in different units, the comparison may provide insight into the TMC materials for hydrogen evolution. Table 1 compares the amount of hydrogen evolution from various transition metal chalcogenides studied under different experimental conditions. It can be clearly seen that different levels of metal doping enhance the hydrogen production, where the carbonaceous substrates improve the performance by providing better surface sites. Further, dye sensitization on these materials and their influence on hydrogen production were also studied. In addition, variable morphologies, such as nanosheets, films, and nanotubes of TMC materials were studied and are illustrated in the table below. Although the com-

parison of different photocatalysts is challenging, it can be clearly seen that the catalyst prepared in this work exhibits a reasonably good amount of hydrogen in addition to better degradation ability.
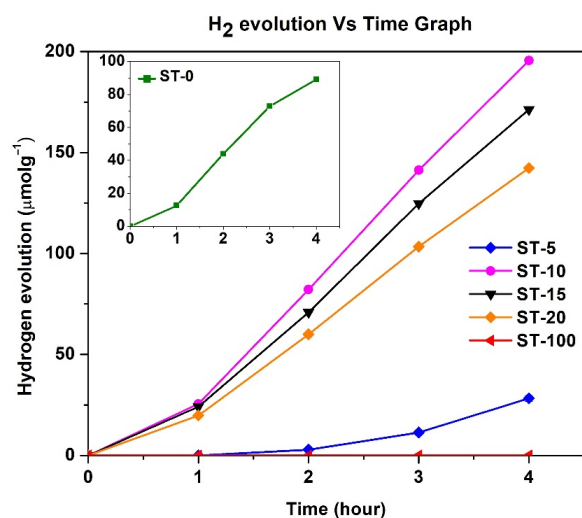

Figure 5. The amount of hydrogen evolved vs. time in the presence of pristine TiO_2, SnS_2, and SnS_2/TiO_2 nanocomposite with different weight percentage (ST-5, ST-10, ST-15, and ST-20) in different time intervals.

Table 1. A comparison of amount of hydrogen evolved with different transition metal chalcogenides.

Material	Preparation Method	Amount of Hydrogen Produced	Ligtht Source	Sacrificial Agent	
CdS on WS_2	Impregnation–sulfidation	0.198 mmolh^{-1}	Visible	Latic acid	[36]
Dye-sensitized NiS_x on graphene	In situ chemical deposition	0.34 mmolh^{-1}	-	-	[9]
MoS_2 on RGO and CdS	Photoreduction	0.099 mmolh^{-1}	Visible	Latic acid	[37]
MoS_2 on graphene	Hydrothermal	1.80 mmolh^{-1}	Visible	Na_2S-$Na_2S_2O_3$	[38]
MoS_2 QDs on TiO_2 NTA	Electrodeposition	0.065 mmolcm^{-2}h^{-1} 0.053 mmolcm^{-2}h^{-1} 0.016 mmolcm^{-2}h^{-1}	UV Visible NIR	-	[19]
ZnTCPP-MoS_2 on TiO_2	Hydrothermal	0.010 mmolh^{-1}	-	triethanolamine (TEOA)	[39]
10 wt. % CoS_2 on TiO_2	Hydrothermal	2.55 mmolg^{-1}	UV	Methanol	[26]
2D SnS_2 on g-C_3N_4	Hydrothermal	0.972 mmolh^{-1}g^{-1}	Visible	TEOA and $H_2Pt_2Cl_6.6H_2O$	[40]
Te/SnS_2/Ag	Hydrothermal	0.332 mmolh^{-1}	UV–visible	-	[41]
SnS_2 nanosheets	Solvothermal	1.06 mmolh^{-1}g^{-1}	UV–visible	Na_2S $Na_2S_2O_3$	[42]
CdS on SnS_2	Hydrothermal	20.2 mmolh^{-1}g^{-1}	UV–visible	Latic acid	[35]
Pt nanoparticles on oxide, Pt nanoparticles on SnS_2 nanoplatelets, and Pt nanoparticles on SnS_2 and oxide	Hydrothermal	10.0 mmolh^{-1}g^{-1} 9.0 mmolh^{-1}g^{-1} 3.0 mmolh^{-1}g^{-1}	UV		[43]
10 wt. % SnS_2 on TiO_2 nanocomposite	Hydrothermal	0.195 mmolg^{-1}	UV–visible	Methanol	

2.3. Photocatalytic Degradation

Photocatalytic degradation of methylene blue was also employed to study the synergic effect of the prepared nanocomposite materials. The reaction suspension was allowed to establish adsorption equilibrium by stirring the suspension in the dark for 30 min. After direct sunlight illumination, the solution withdrawn from the reactor in a time interval was tested by studying the absorbance of the remnant dye solution. The absorption spectra for different samples, such as (a) pure TiO_2 (ST-0), (b) pure SnS_2 (ST-100), SnS_2/TiO_2 nanocomposites ((c) ST-5, (d) ST-10, (e) ST-15, and (f) ST-20 are illustrated in Figure 6, which clearly explains the better photocatalytic activity of these nanocomposites. The rate of the reaction was determined by the linear plot of ln (A/A_0) vs. time A_0-absorbance of initial solution ($t = 0$), where A is absorption of the solution at time t. The highest rate of degradation was obtained for the sample ST-15 (15 wt. % of SnS_2/TiO_2) with the rate of 4.415×10^{-4} s^{-1} compared to the pure TiO_2 (2.745×10^{-4} s^{-1}) and SnS_2 (1.955×10^{-4} s^{-1}). These results may suggest the essential role of SnS_2 in the nanocomposite photocatalyst, which enhances the separation of photo-generated electron–hole pairs and thus maximizes the utilization of photon under direct sunlight. It is well known that there are two possible paths for the degradation of the dye: (i) the visible light can be absorbed by the dye molecules, resulting in excited electrons and injection of these electrons into the conduction band of the catalyst, and (ii) the catalyst itself can absorb photons, and the electrons ejected from the valence band to the conduction band will then migrate to its active site. Further, in this study, the scavenging experiments were conducted in the presence of an N_2 environment (absence of O_2) and in the presence of IPA (to scavenge the $\bullet$OH radical). It can be clearly seen that there was a 78% reduction in the rate when IPA was used as the scavenger (Figure S3, Supplementary Materials), whereas around 95% reduction was attained while N_2 was used as the scavenger (Figure S4, Supplementary Materials). Notably, very low degradation (<5%) was attained when the dye alone was placed under direct light (Figure S5, Supplementary Materials). These results further validate that the $\bullet$OH radical and the superoxide radicals ($^{\bullet}O_2$) can be acknowledged in the degradation mechanism of MB (Figure 7). The effective degradation efficiency can be attributed to the combined effect of in situ dye sensitization and the impregnation of chalcogenide materials on TiO_2.
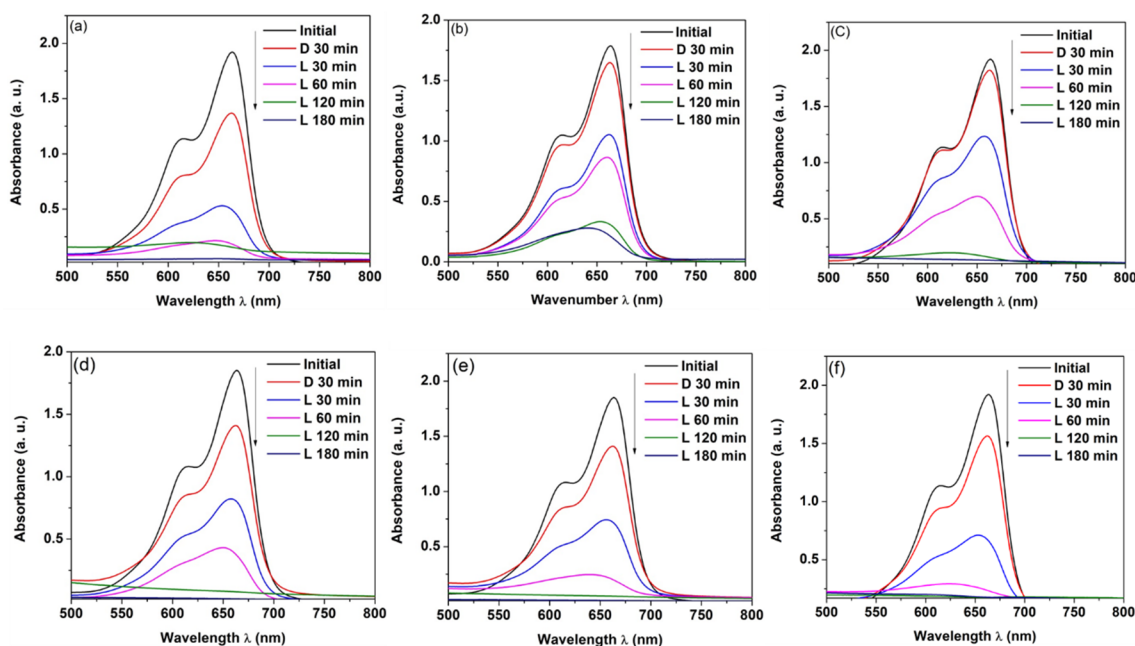

Figure 6. Absorbance vs. wavelength graph for degradation of methylene blue by using pristine (**a**) TiO_2 (ST-0), (**b**) SnS_2 (ST-100) and SnS_2/TiO_2 nanocomposites (**c**) ST-5, (**d**) ST-10, (**e**) ST-15 and (**f**) ST-20 as photocatalysts at different time intervals under direct sunlight.
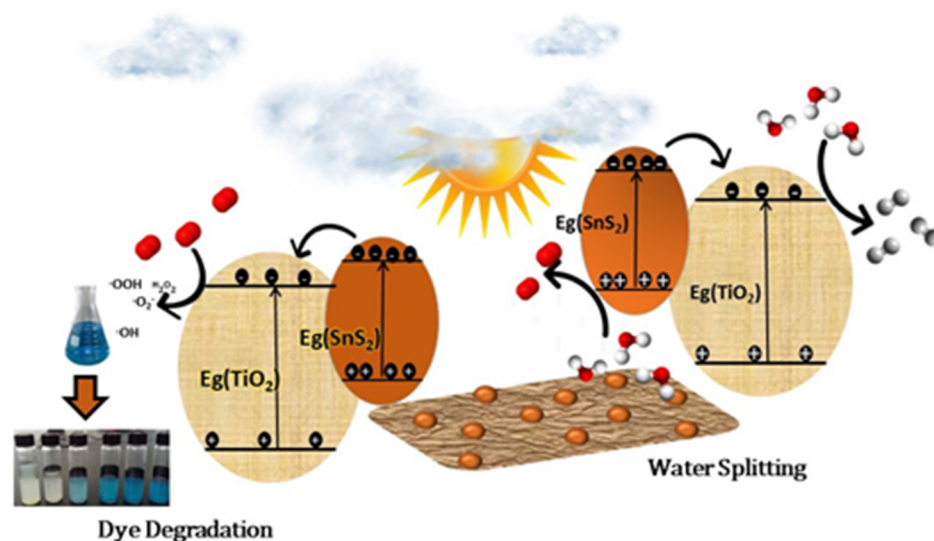
Figure 7. Photocatalytic mechanism.

A comparison between the rate of degradation and the hydrogen production is listed in Table 2. As indicted in the table, the bandgap energy of the materials can be correlated with the better performance of degradation and hydrogen production. The materials ST-10 and ST-15 show very similar bandgaps, and that may be attributed to the higher performance of those materials. The replication studies also showed a similar trend in the photocatalytic degradation and hydrogen production.

Table 2. Comparison of the amount of hydrogen evolved and rate constant of the degradation reaction of MB by using pure SnS_2, TiO_2, and SnS_2-embedded TiO_2 nanocomposite over simulated irradiation with the bandgap of these materials.

Sample	Amount of Hydrogen Evolved ($\mu mol g^{-1}$)	Rate Constant of Photodegradation Reaction ($\times 10^{-4}$ s^{-1})	Calculated BandGap Value (eV)
ST-100	0.00	1.955 ± 0.185	1.890
ST-20	142.35	2.768 ± 0.181	1.980
ST-15	171.30	4.415 ± 0.258	2.005
ST-10	195.55	3.948 ± 0.110	2.015
ST-5	28.25	2.661 ± 0.388	2.250
ST-0	89.20	2.745 ± 0.513	3.100

3. Materials and Methods

3.1. Materials

The following chemicals were used without further purification. Titanium tetra iso-propoxide, 98+% (Sigma–Aldrich Norway AS, Oslo, Norway) was employed as the precursor for TiO_2 preparation. Concentrated HNO_3 (Sigma–Aldrich Norway AS) PHARMCO-AAPER ethyl alcohol (200 proof; absolute, anhydrous, Sigma–Aldrich Norway AS) was used as catalyst and solvent, respectively. Tin (II) chloride, pentahydrate, ACS reagent, ≥98% (Sigma–Aldrich Norway AS) was used as the tin precursor; thiourea, ACS reagent, 99.0% (Sigma–Aldrich Norway AS) was utilized as sulfur source; and conc. HCl (used as hydrolyzer) and deionized water (resistivity > 18 M cm, Velp/AREC, VELP Scientifica Srl, Usmate, MB, Italy) were used to prepare the solution mixtures.

3.2. Methods

3.2.1. Synthesis

Titanium Dioxide

Nanocrystalline titanium dioxide was prepared using the method we reported previously [26] under hydrothermal conditions using the sol–gel technique. In a typical synthesis, 32.5 mL of ethanol is acidified with 0.3 mL concentrated HNO_3 in a Teflon liner and stirred at a constant speed (300 rpm); 6.60 mL of titanium (iv) isopropoxide is then added drop wise into it with continuous stirring; finally, 3.0 mL of water is added to the solution for the formation of a gel. It is then transferred into an autoclave (AUTOCLAVE-PTFE-0100, TECINSTRO, Maharashtra, India) and kept at 180 °C for 6 h. The final product is then washed with ethanol, and the dried product calcined at 500 °C for 6 h.

SnS_2-Embedded TiO_2 Nanocomposite

The appropriate amount of $SnCl_2.2H_2O$ was taken into a 50 mL beaker containing 0.8 mL of concentrated hydrochloric acid (37%) in 10 mL of deionized water. It was then stirred at 300 rpm for 30 min, followed by the addition of the appropriate amount of TiO_2 (hydrothermally synthesized) before being completely dispersed by constant stirring for 10 min. Then, an appropriate amount of thiourea was added into the solution made up to 40 mL volume by adding deionized water. Finally, the resulting solution was transferred in an autoclave and kept at 145 °C for 12 h. The final product was collected by centrifugation, and it was washed with the mixture of deionized water and ethanol (v/v = 1:1) several times. It was then air-dried to prepare X wt. % (X = 0 (ST-0), 5 (ST-5), 10 (ST-10), 15 (ST-15), 20 (ST-20), and 100 (ST-100)) of the SnS_2-embedded TiO_2 material. Similar conditions were followed in the preparation of pristine SnS_2 nanoparticles without adding titanium dioxide. We refer to this as ST-0—SnS_2 is denoted by S; T stands for TiO_2; and the numbers 0, 5, 10, 15, 20, and 100 are the wt. % of SnS_2 in TiO_2.

3.2.2. Characterization

Synthesized nanocomposite materials were characterized using different techniques, such as powder X-ray diffraction (patterns of the catalysts were recorded using D8 AD-VANCE ECO in a 1 kW copper X-ray tube diffractometer with the scan range from 3 to 90 degrees (2theta)), diffuse reflectance spectra (DRS Cary 100 Bio UV-Visible spectrophotometer, Santa Clara, CA, USA) by measuring the intensity in the wavelength range of 800–200 nm, and scanning electron microscopy (SEM, Oxford instrument, Nano Analysis, Concord, MA, USA).

3.2.3. Photocatalytic Hydrogen Evolution

The photocatalytic experiments were carried out for pristine TiO_2, SnS_2, and ST-X (X = 05, 10, 15, and 20). Firstly, the synthesized nanocomposite was suspended in a solution containing 1.5 mL of deionized water and 0.5 mL of methanol (hole scavenger). The suspension was degassed for 30 min with high-purity argon prior to irradiation. The final suspensions were continuously stirred throughout the experiment. A 300 W Xenon lamp (Oriel light source, Xenon arc lamp, Newport 1000W, Irvine, CA, USA) with an AM 1.5 G filter was used as the source of radiation. Finally, the amount of H_2 produced was measured by using gas chromatography (SRI 8610 C, SRI Instruments, Torrance, CA, USA) equipped with a molecular sieve column and a TCD (thermal conductivity detector), and the amount of hydrogen produced was quantified by using a calibration curve prepared previously.

3.2.4. Photocatalytic Degradation

Photocatalytic degradation of methylene blue (MB) solution was performed using a ST-X nanocomposite photocatalyst. In a typical experiment, 25.0 mg of the photocatalyst is suspended with 50 mL of MB solution (initial concentration of 10 ppm) under direct sunlight. Prior to irradiation, the suspensions are sonicated in the dark for 30 min to ensure the establishment of adsorption or desorption equilibrium. Periodically, 3 mL of

suspension is withdrawn, and absorption spectra of the solution are obtained using a UV/Vis spectrometer (JENWAY 6800 UV/Vis spectrophotometer (OSA, UK)). Scavenging experiments were also carried out under the IPA and N_2 environment.

4. Conclusions

The pure SnS_2, TiO_2, and different wt. % of SnS_2/TiO_2 nanocomposite samples were successfully synthesized by the facile hydrothermal process, affording an effective photocatalyst that can be utilized for hydrogen production and degradation of methylene blue. The SnS_2/TiO_2 nanocomposite with 10 wt. % shows an optimum rate of hydrogen production of 195.55 $\mu molg^{-1}$, whereas SnS_2/TiO_2 nanocomposites with 15 wt. % exhibit a high rate of degradation of methylene blue (4.415×10^{-4} s^{-1}). The pure SnS_2 was found to be inactive due to a lower bandgap, and pure TiO_2 shows less photoactivity compared with the nanocomposites. This study concludes that SnS_2 acts as co-catalyst and thus effectively induces the formation of electron–hole pairs that leads to the higher photocatalytic activity in both hydrogen production and photodegradation applications. The scavenging experiments showed evidence of a 78% reduction in the rate of degradation when IPA was used as the scavenger, whereas around 95% reduction was attained in the presence of N_2. Nearly no (<5%) degradation was attained when the dye alone was under direct solar irradiation. Furthermore, our analysis clearly showed that enhancement in degradation MB could be attributed to hydroxyl radicals and superoxide radicals.

References

1. Ran, J.; Zhang, J.; Yu, J.; Jaroniec, M.; Qiao, S.Z. Earth-abundant cocatalysts for semiconductor-based photocatalytic water splitting. *Chem. Soc. Rev.* **2014**, *43*, 7787–7812. [CrossRef]
2. Nguyen, P.D.; Duong, T.M.; Tran, P.D. Current progress and challenges in engineering viable artificial leaf for solar water splitting. *J. Sci. Adv. Mater. Devices* **2017**, *2*, 399–417. [CrossRef]
3. Leung, D.Y.C.; Fu, X.; Wang, C.; Ni, M.; Leung, M.K.H.; Wang, X.; Fu, X. Hydrogen production over titania-based photocatalysts. *ChemSusChem* **2010**, *3*, 681–694. [CrossRef]
4. Yin, Y.; Jin, Z.; Hou, F. Enhanced solar water-splitting efficiency using core/sheath heterostructure CdS/TiO₂ nanotube arrays. *Nanotechnology* **2007**. [CrossRef] [PubMed]
5. Kim, S.B.; Hong, S.C. Kinetic study for photocatalytic degradation of volatile organic compounds in air using thin film TiO₂ photocatalyst. *Appl. Catal. B Environ.* **2002**, *35*, 305–315. [CrossRef]
6. Rasalingam, S.; Peng, R.; Koodali, R.T. Removal of Hazardous Pollutants from Wastewaters: Applications of TiO₂-SiO₂ Mixed Oxide Materials Shivatharsiny. *J. Nanomater.* **2014**, *2014*, 617405. [CrossRef]
7. Chakrabarti, S.; Dutta, B.K. Photocatalytic degradation of model textile dyes in wastewater using ZnO as semiconductor catalyst. *J. Hazard. Mater.* **2004**, *112*, 269–278. [CrossRef]

8.   Mugunthan, E.; Saidutta, M.B.; Jagadeeshbabu, P.E. Photocatalytic degradation of diclofenac using TiO$_2$–SnO$_2$ mixed oxide catalysts. *Environ. Technol.* **2019**, *40*, 929–941. [CrossRef]

9.   Kong, C.; Min, S.; Lu, G. Dye-sensitized NiS$_x$ catalyst decorated on graphene for highly efficient reduction of water to hydrogen under visible light irradiation. *ACS Catal.* **2014**, *4*, 2763–2769. [CrossRef]

10. Pirashanthan, A.; Murugathas, T.; Mariappan, K.; Ravirajan, P.; Velauthapillai, D.; Yohi, S. A multifunctional ruthenium based dye for hybrid nanocrystalline titanium dioxide/poly(3-hexylthiophene) solar cells. *Mater. Lett.* **2020**, *274*, 127997. [CrossRef]

11. Zhang, W.; Xiao, X.; Zeng, X.; Li, Y.; Zheng, L.; Wan, C. Enhanced photocatalytic activity of TiO$_2$ nanoparticles using SnS$_2$/RGO hybrid as co-catalyst: DFT study and photocatalytic mechanism. *J. Alloys Compd.* **2016**, *685*, 774–783. [CrossRef]

12. Jafari, T.; Moharreri, E.; Amin, A.S.; Miao, R.; Song, W.; Suib, S.L. Photocatalytic water splitting—The untamed dream: A review of recent advances. *Molecules* **2016**, *21*, 900. [CrossRef] [PubMed]

13. Pirashanthan, A.; Murugathas, T.; Robertson, N.; Ravirajan, P.; Velauthapillai, D. A Quarterthiophene-Based Dye as an Efficient. *Polymers* **2019**, *11*, 1752. [CrossRef]

14. Eidsvåg, H.; Bentouba, S.; Vajeeston, P.; Yohi, S.; Velauthapillai, D. TiO$_2$ as a Photocatalyst for Water Splitting—An Experimental and Theoretical Review. *Molecules* **2021**, *26*, 1687. [CrossRef] [PubMed]

15. Rajaramanan, T.; Natarajan, M.; Ravirajan, P.; Senthilnanthanan, M.; Velauthapillai, D. Ruthenium (Ru) Doped Titanium Dioxide (P25) electrode for dye sensitized solar cells. *Energies* **2020**, *13*, 1532. [CrossRef]

16. Li, Y.; Zhou, X.; Xing, Y. In situ thermal-assisted loading of monodispersed Pt nanoclusters on CdS nanoflowers for efficient photocatalytic hydrogen evolution. *Appl. Surf. Sci.* **2020**, *506*, 144933. [CrossRef]

17. Shanmugaratnam, S.; Rasalingam, S. Transition Metal Chalcogenide (TMC) Nanocomposites for Environmental Remediation Application over Extended Solar Irradiation. *Intech* **2019**. [CrossRef]

18. Zheng, L.; Zhang, W.; Xiao, X. Preparation of titanium dioxide/tungsten disulfide composite photocatalysts with enhanced photocatalytic activity under visible light. *Korean J. Chem. Eng.* **2016**, *33*, 107–113. [CrossRef]

19. Wang, Q.; Huang, J.; Sun, H.; Ng, Y.H.; Zhang, K.Q.; Lai, Y. MoS$_2$ Quantum Dots@TiO$_2$ Nanotube Arrays: An Extended-Spectrum-Driven Photocatalyst for Solar Hydrogen Evolution. *ChemSusChem* **2018**, *11*, 1708–1721. [CrossRef]

20. Meng, Z.; Oh, W. Photodegradation of Organic Dye by CoS$_2$ and Carbon(C60, Graphene, CNT)/TiO$_2$ Composite Sensitizer. *Chin. J. Catal.* **2012**, *33*, 1495–1501. [CrossRef]

21. Kajana, T.; Velauthapillai, D.; Shivatharsiny, Y.; Ravirajan, P.; Yuvapragasam, A.; Senthilnanthanan, M. Structural and photoelectrochemical characterization of heterostructured carbon sheet/Ag$_2$MoO$_4$-SnS/Pt photocapacitor. *J. Photochem. Photobiol. A Chem.* **2020**, *401*, 112784. [CrossRef]

22. Chen, T.Y.; Chang, Y.H.; Hsu, C.L.; Wei, K.H.; Chiang, C.Y.; Li, L.J. Comparative study on MoS$_2$ and WS$_2$ for electrocatalytic water splitting. *Int. J. Hydrog. Energy* **2013**, *38*, 12302–12309. [CrossRef]

23. Ali, A.; Oh, W.C. Photocatalytic performance of CoS$_2$-graphene-TiO$_2$ ternary composites for reactive black B (RBB) degradation. *J. Korean Ceram. Soc.* **2017**, *54*, 308–313. [CrossRef]

24. Li, Y.; Wang, H.; Xie, L.; Liang, Y.; Hong, G.; Dai, H. MoS$_2$ nanoparticles grown on graphene: An advanced catalyst for the hydrogen evolution reaction. *J. Am. Chem. Soc.* **2011**, *133*, 7296–7299. [CrossRef] [PubMed]

25. He, K.; Xie, J.; Li, M.; Li, X. In situ one-pot fabrication of g-C$_3$N$_4$ nanosheets/NiS cocatalyst heterojunction with intimate interfaces for efficient visible light photocatalytic H$_2$ generation. *Appl. Surf. Sci.* **2018**, *430*, 208–217. [CrossRef]

26. Shanmugaratnam, S.; Velauthapillai, D.; Ravirajan, P.; Christy, A.A.; Shivatharsiny, Y. CoS$_2$/TiO$_2$ in nanocomposites for hydrogen production under UV irradiation. *Materials* **2019**, *12*, 3882. [CrossRef] [PubMed]

27. Khan, Z.; Chetia, T.R.; Vardhaman, A.K.; Barpuzary, D.; Sastri, C.V.; Qureshi, M. Visible light assisted photocatalytic hydrogen generation and organic dye degradation by CdS-metal oxide hybrids in presence of graphene oxide. *RSC Adv.* **2012**, *2*, 12122–12128. [CrossRef]

28. Sun, B.; Liu, A.; Li, J.; Wang, J.; Wang, S. Development of novel highly stable synergistic quaternary photocatalyst for the efficient hydrogen evolution reaction. *Appl. Surf. Sci.* **2020**, *510*, 145498. [CrossRef]

29. Zhu, W.; Yang, Y.; Ma, D.; Wang, H.; Zhang, Y.; Hu, H. Controlled growth of flower-like SnS$_2$ hierarchical structures with superior performance for lithium-ion battery applications. *Ionics* **2014**, *21*, 19–26. [CrossRef]

30. Mondal, C.; Ganguly, M.; Pal, J.; Roy, A.; Jana, J.; Pal, T. Morphology controlled synthesis of SnS$_2$ nanomaterial for promoting photocatalytic reduction of aqueous Cr(VI) under visible light. *Langmuir* **2014**, *30*, 4157–4164. [CrossRef]

31. Gaur, R.; Jeevanandam, P. Synthesis of SnS$_2$ nanoparticles and their application as photocatalysts for the reduction of Cr(VI). *J. Nanosci. Nanotechnol.* **2018**, *18*, 165–177. [CrossRef]

32. Feng, J.; Chen, J.; Geng, B.; Feng, H.; Li, H.; Yan, D.; Zhuo, R.; Cheng, S.; Wu, Z.; Yan, P. Two-dimensional hexagonal SnS$_2$ nanoflakes: Fabrication, characterization, and growth mechanism. *Appl. Phys. A Mater. Sci. Process.* **2011**, *103*, 413–419. [CrossRef]

33. Geng, H.; Su, Y.; Wei, H.; Xu, M.; Wei, L.; Yang, Z.; Zhang, Y. Controllable synthesis and photoelectric property of hexagonal SnS$_2$ nanoflakes by Triton X-100 assisted hydrothermal method. *Mater. Lett.* **2013**, *111*, 204–207. [CrossRef]

34. Rasalingam, S.; Wu, C.M.; Koodali, R.T. Modulation of pore sizes of titanium dioxide photocatalysts by a facile template free hydrothermal synthesis method: Implications for photocatalytic degradation of rhodamine B. *ACS Appl. Mater. Interfaces* **2015**, *7*, 4368–4380. [CrossRef]

35. Rangappa, A.P.; Kumar, D.P.; Gopannagari, M.; Reddy, D.A.; Hong, Y.; Kim, Y.; Kim, T.K. Highly efficient hydrogen generation in water using 1D CdS nanorods integrated with 2D SnS$_2$ nanosheets under solar light irradiation. *Appl. Surf. Sci.* **2020**, *508*, 144803. [CrossRef]

36. Zong, X.; Han, J.; Ma, G.; Yan, H.; Wu, G.; Li, C. Photocatalytic H_2 evolution on CdS loaded with WS_2 as cocatalyst under visible light irradiation. *J. Phys. Chem. C* **2011**, *115*, 12202–12208. [CrossRef]

37. Li, Y.; Wang, H.; Peng, S. Tunable photodeposition of MoS_2 onto a composite of reduced graphene oxide and CdS for synergic photocatalytic hydrogen generation. *J. Phys. Chem. C* **2014**, *118*, 19842–19848. [CrossRef]

38. Chang, K.; Mei, Z.; Wang, T.; Kang, Q.; Ouyang, S.; Ye, J. MoS_2/graphene cocatalyst for efficient photocatalytic H_2 evolution under visible light irradiation. *ACS Nano* **2014**, *8*, 7078–7087. [CrossRef]

39. Yuan, Y.; Lu, H.; Ji, Z.; Zhong, J.; Ding, M.; Chen, D.; Li, Y.; Tu, W.; Cao, D.; Yu, Z.; et al. Enhanced visible-light-induced hydrogen evolution from water in a noble-metal-free system catalyzed by ZnTCPP-MoS_2/TiO_2 assembly. *Chem. Eng. J.* **2015**, *275*, 8–16. [CrossRef]

40. Liu, E.; Chen, J.; Ma, Y.; Feng, J.; Jia, J.; Fan, J.; Hu, X. Fabrication of 2D SnS_2 /g-C_3N_4 heterojunction with enhanced H_2 evolution during photocatalytic water splitting. *J. Colloid Interface Sci.* **2018**, *524*, 313–324. [CrossRef] [PubMed]

41. Yan, C.; Xue, X.; Zhang, W.; Li, X.; Liu, J.; Yang, S.; Hu, Y.; Chen, R.; Yan, Y.; Zhu, G.; et al. Well-designed Te/SnS_2/Ag artificial nanoleaves for enabling and enhancing visible-light driven overall splitting of pure water. *Nano Energy* **2017**, *39*, 539–545. [CrossRef]

42. Yu, J.; Xu, C.Y.; Ma, F.X.; Hu, S.P.; Zhang, Y.W.; Zhen, L. Monodisperse SnS_2 nanosheets for high-performance photocatalytic hydrogen generation. *ACS Appl. Mater. Interfaces* **2014**, *6*, 22370–22377. [CrossRef] [PubMed]

43. Barba-Nieto, I.; Christoforidis, K.C.; Fernández-García, M.; Kubacka, A. Promoting H_2 photoproduction of TiO_2-based materials by surface decoration with Pt nanoparticles and SnS_2 nanoplatelets. *Appl. Catal. B Environ.* **2020**, *277*, 119246. [CrossRef]